Article

Comprehensive Schottky Barrier Height Behavior and Reliability Instability with Ni/Au and Pt/Ti/Pt/Au on AlGaN/GaN High-Electron-Mobility Transistors

Surajit Chakraborty (ID) **and Tae-Woo Kim** *(ID)

Department of Electrical, Electronic and Computer Engineering, University of Ulsan, Ulsan 44610, Korea; surajit5103@ulsan.ac.kr
* Correspondence: twkim78@ulsan.ac.kr

Abstract: The reliability instability of inhomogeneous Schottky contact behaviors of Ni/Au and Pt/Ti/Pt/Au gate contacts on AlGaN/GaN high-electron-mobility transistors (HEMTs) was investigated via off-state stress and temperature. Under the off-state stress condition, Pt/Ti/Pt/Au HEMT showed abruptly reduced reverse leakage current, which improved the Schottky barrier height (SBH) from 0.46 to 0.69 eV by suppression of the interfacial donor state. As the temperature increased, the reverse leakage current of the Pt/Ti/Pt/Au AlGaN/GaN HEMT at 308 K showed more reduction under the same off-state stress condition while that of the Ni/Au AlGaN/GaN HEMT increased. However, with temperatures exceeding 308 K under the same off-state stress conditions, the reverse leakage current of the Pt/Ti/Pt/Au AlGaN/GaN HEMT increases, which can be intensified using the inverse piezoelectric effect. Based on this phenomenon, the present work reveals the necessity for analyzing the concurrent SBH and reliability instability due to the interfacial trap states of the MS contacts.

Keywords: AlGaN/GaN; critical voltage; degradation; off-state stress; inverse piezoelectric effect; high temperature; Schottky barrier height; reliability instability

1. Introduction

Gallium nitride (GaN)-based high-electron-mobility transistors (HEMTs) have attracted attention in microwave and power-switching applications due to their unparalleled properties including wide direct bandgap, high-temperature operation, high breakdown field, and high-saturation electron velocity [1–3]. Because of piezoelectric and spontaneous polarizations in AlGaN/GaN, GaN-based HEMTs have been used to achieve high carrier densities and high mobilities at the heterostructure without doping by the origination of two-dimensional electron gas (2DEG) channels [4–6]. The electrical performances of GaN-based HEMT devices show sturdy functions of both Schottky and Ohmic metal contacts because the Schottky contact in AlGaN/GaN is controlled by the current conduction in the channel [7]. The gate reverse leakage current still remains a key concern for GaN-HEMT stability due to the interfacial trap states and strain-induced defects such as dislocations and cracks from large lattice mismatches [8–12]. Severe limitations such as current collapse, power slump, and poor long-term reliability are induced by the trapping effects at the interfacial trap states, trap sites in the AlGaN barrier layer, and deep-level traps in the GaN buffer layer [13–15].

In particular, trapping characteristics were evaluated to reduce the density of states for the surface donors using different gate metals on the AlGaN/GaN heterostructure [16,17]. One of the solutions proposed for such GaN-based HEMTs is the improvement in the interactions between the metal and semiconductor surfaces mediated by dangling bonds [18]. Schottky contacts on GaN and AlGaN/GaN heterostructures have been investigated for various metals including Pt, Au, Ti, Ni, Au, and other highly heat resistant metals [19–21].

Despite the excellent tuning of the Schottky barrier height (SBH) on a GaN-based HEMT, the reliability instability remains a primary concern for device optimization due to the relationships between the qualities of the AlGaN/GaN epitaxial layers and their geometries [22]. In particular, the carriers in the GaN channel can achieve high energies at the gate edge on the drain side, where the combined injection velocity from the lateral and vertical directions is the maximum [23]. The degradation of the hot carriers may cause a significant reduction in the drain current and transconductance (Gm) as well as shifts in the threshold voltage (VT), resulting in decreased direct current (DC), radio frequency (RF), and large-signal performances [24,25]. To quantitatively understand the electrostatic characteristics of the AlGaN/GaN heterostructure, it is necessary to comprehensively analyze the concurrent SBH and reliability instability due to the interfacial trap states of the metal–semiconductor (MS) contacts.

In this study, we investigated the comprehensive SBH and temperature as well as device degradation of Ni/Au and Pt/Ti/Pt/Au contacts on AlGaN/GaN HEMTs. The Schottky behavior characteristics for the Ni/Au and Pt/Ti/Pt/Au gate were compared, and the thermal reliability instability was examined at elevated temperatures. There are many studies [26–31] on the reliability of the Ni and Pt gated structure, but our experimental method is unique and revived the property of Pt metal into its original condition.

2. Materials and Methods

The epitaxial layer structures were grown via the low-pressure metal-organic chemical vapor deposition (MOCVD) technique on 3-inch p-type Si wafers. This epitaxial structure consists of an $Al_{0.21}Ga_{0.79}N$ barrier (28.5 nm), a Ga-polarity GaN channel layer (50 nm), and an AlGaN intermediate buffer layer (200 nm) atop the 3-inch p-Si substrate. Hall measurements revealed the mobility (μ_{n_Hall}) and the sheet charge density (2DEG) to be 1300 $cm^2 \cdot V^{-1} \cdot s^{-1}$ and 9×10^{12} cm^{-2}, respectively. The device fabrication involved mesa isolation etching, source/drain ohmic contact formation, and gate patterning. The mesa isolation etching was performed using a reactive ion etching (RIE) system; thereafter, the ohmic contacts were formed by standard Ti/Al/Ni/Au (25/160/40/100 nm) metallization on the source and drain regions, followed by rapid thermal annealing (RTA) at 830 °C for 30 s in ambient N_2 to allow for the formation of the contacts on the AlGaN/GaN epistructure. The contact resistance (R_c) and sheet resistance (R_{SH}) extracted by transmission-line-method (TLM) measurements were 1.2 Ω·mm and 320 Ω/□, respectively. Metallization was performed via the lift-off technique. The Schottky gate contacts were next patterned by photolithography; the Ni/Au (20/300 nm) and Pt/Ti/Pt/Au (8/20/20/300 nm) Schottky gate contacts were fabricated by e-beam evaporation, and Al_2O_3 (3 nm) was deposited as the surface passivation layer. A schematic cross-sectional structure and two different gate metals are shown in Figure 1a,b respectively. To understand the roles of the temperature and Schottky behavior characteristics, the electrical performance, I–V (current-voltage) characteristics, and C–V (capacitance–voltage) measurements were evaluated using a Keithley 4200SC semiconductor parameter analyzer and 4210-CVU, which were connected to a probe station with a temperature-controlled (Temptronic TP03000) heating plate.

The critical voltage was determined via incrementally stepped stress values of the V_G from −10 V, with the source and drain terminals grounded to avoid self-heating. At each stress step, similar gate length devices from each wafer were stressed for 1 min. To verify the degradation of the SBH under the off-state stress, a constant stress condition ($V_D = 50$ V, $V_G = -7$ V) was applied over a duration of 1 h to the gate and drain regions, with the source being grounded. To investigate the temperature dependence under the off-state stress, both devices, with the same gate length of Lg = 10 μm, were stressed at constant voltage ($V_D = 50$ V, $V_G = -7$ V) for 1 h by increasing the temperature from 298 K to 368 K in steps of 10 K. In our study, due to high gate leakage current, the calculation of the ideality factor did not provide satisfactory results for a gate length of 14 μm. Therefore, we considered a lower gate length of 10 μm to investigate the Schottky barrier degradation

effect in both the temperature and stress related experiments. More than 35 devices with different gate lengths (10 μm, 11 μm, and 14 μm) were used in this study.

(a)   **(b)**
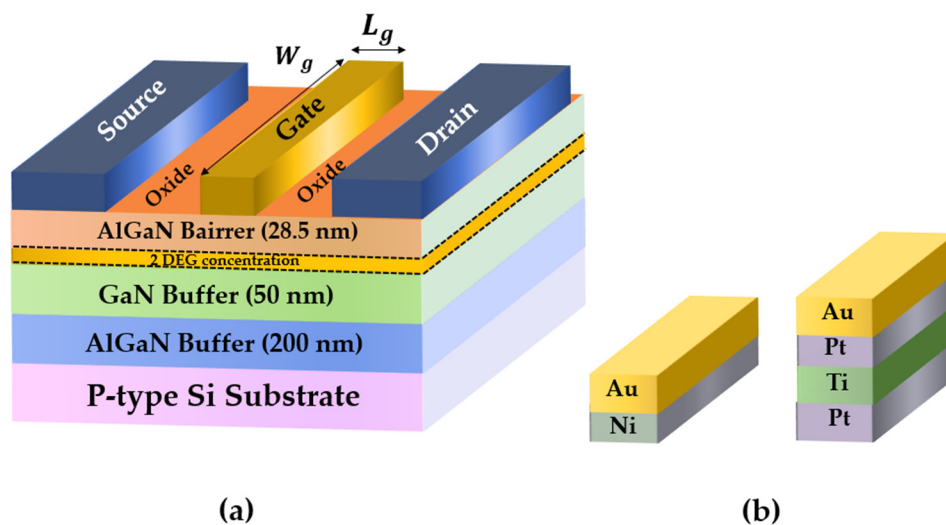
Figure 1. (**a**) Schematic cross section showing Ni/Au and Pt/Ti/Pt/Au gate contacts on the AlGaN/GaN HEMT. The Schottky gate contact on the AlGaN/GaN HEMT controls the current conduction in the GaN channel. (**b**) Gate metal stack for two different HEMTs.

3. Results and Discussion

3.1. Impact of Schottky Contact Electrodes on Electrical Properties

Figure 2a–c shows the I–V characteristics of both the forward and reverse region, and Schottky characteristics (J–V characteristics) of the Ni/Au and Pt/Ti/Pt/Au Schottky contacts on the AlGaN/GaN HEMTs, respectively. In Figure 2a, the Ni/Au Schottky contact showed a forward current of 2.13 A/mm at 5 V while Pt/Ti/Pt/Au showed 0.5 A/mm. The high Schottky barrier height of the contact may cause a reduction in forward current [32]. In the reverse region (Figure 2b), the Pt/Ti/Pt/Au device degraded and showed higher leakage current 6.04×10^{-5} A/mm at −10 V than Ni/Au (5.29×10^{-6} A/mm). The SBHs and ideality factors for the Ni/Au and Pt/Ti/Pt/Au AlGaN/GaN HEMTs are given by (1) and (2), respectively:

$$J = J_S \left[\exp\left(\frac{qV}{nkT} \right) - 1 \right] \tag{1}$$

$$J_S = A^* T^2 \exp\left(\frac{-q\phi_b}{kT} \right) \tag{2}$$

where J_S is the reverse saturation current density; n is the ideality factor; A^* is the effective Richardson constant; T is the absolute temperature; ϕ_b is the SBH obtained from the saturation current density; and k is the Boltzmann constant [33]. The SBH of the Pt/Ti/Pt/Au contact at the reverse-biased region was observed to deteriorate, implying that the surface roughness caused by the high-energy Pt atoms deposited during e-beam evaporation process on the AlGaN/GaN HEMTs ultimately caused cracks in the MS contacts. This phenomenon can be attributed to the inhomogeneities at the MS interface and large deviations in the behaviors of the top electrodes despite the higher work function of Pt compared with Ni. Hence, the reverse leakage current of the Pt/Ti/Pt/Au Schottky contact was higher than that of the Ni/Au contact, as shown in Figure 2.
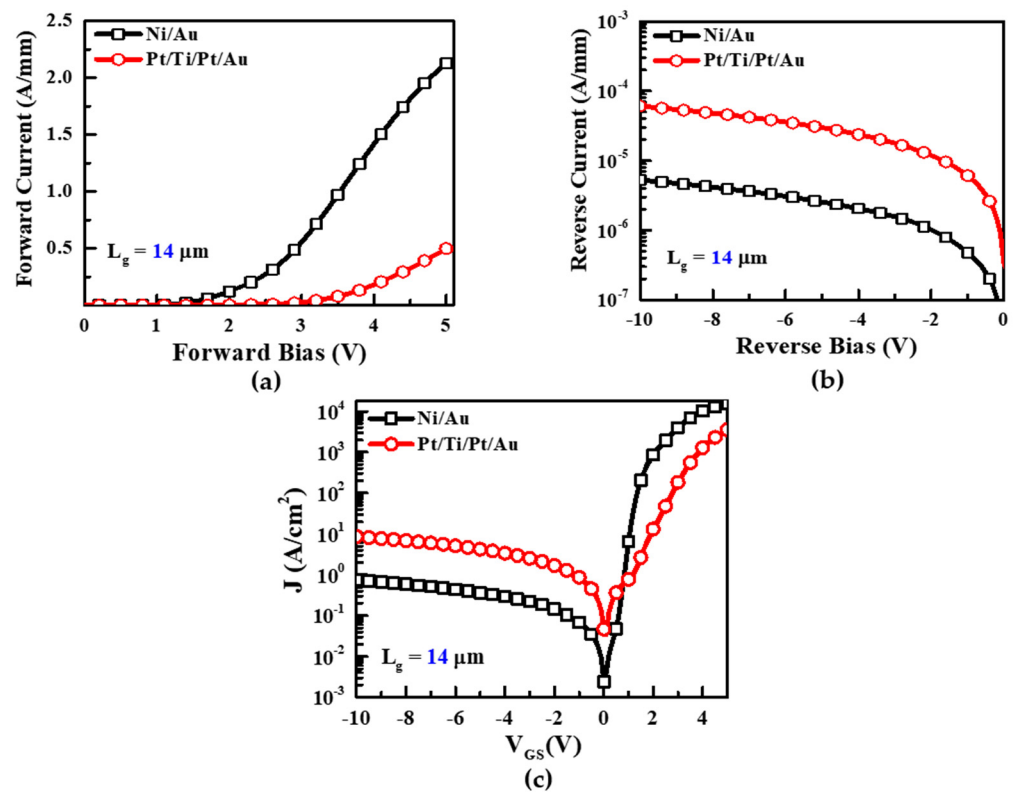
Figure 2. (**a**) Current–voltage plot (I–V) plot (characteristics) of the forward region and (**b**) reverse region. (**c**) Schottky characteristics of the contacts made of Ni/Au and Pt/Ti/Pt/Au fabricated on AlGaN/GaN HEMTs at room temperature.

The capacitance–voltage (C–V) and conductance–voltage (G–V) characteristics of the Ni/Au and Pt/Ti/Pt/Au contacts on the AlGaN/GaN HEMTs were examined at 1 MHz, as shown in Figure 3. The threshold voltage of the Pt/Ti/Pt/Au Schottky contact in the forward region was observed to have a more positive shift of 0.28 V, as shown in Figure 3a. This means that the 2DEG carrier concentration below the Pt/Ti/Pt/Au Schottky contact was significantly reduced due to greater depletion under the Pt/Ti/Pt/Au contact than the Ni/Au contact, thereby indicating that a top electrode made of Pt has a higher work function than that made of Ni [7]. The conductance of the Pt-based Schottky contact was higher in the off region than that of the Ni/Au Schottky contact, indicating the degradation of the off-state leakage current.
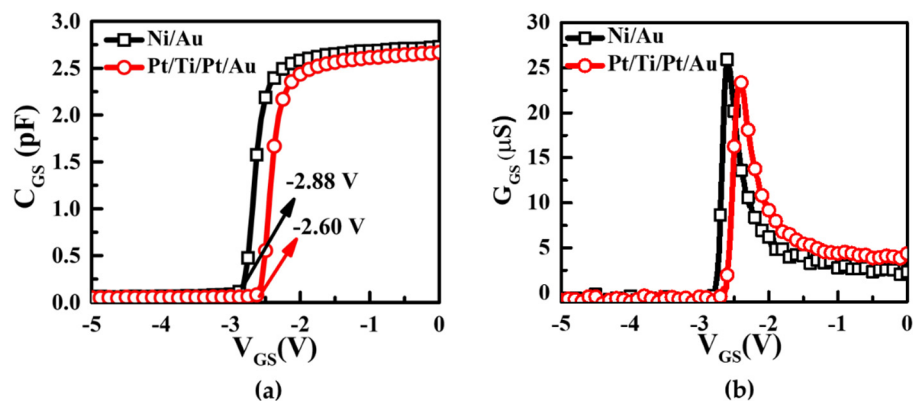

Figure 3. (**a**) Capacitance–voltage (C–V) and (**b**) conductance–voltage (G–V) characteristics of the Ni/Au and Pt/Ti/Pt/Au contacts on AlGaN/GaN HEMTs measured at 1 MHz; the Pt-based Schottky contact was observed to have a more positive shift.

The initial value (before stress) of the Schottky contact calculated both I–V and C–V methods. We measured the C–V characteristics of both devices at 1 MHz at room temperature (Figure 3a). The below equation demonstrated a Schottky barrier relation with capacitance characteristics [33].

$$\frac{A^2}{C^2} = \frac{2\left(V_{bi} - \frac{kT}{q} - V\right)}{qN_D\varepsilon_s} \tag{3}$$

where ϵ_s is the semiconductor permittivity; V_{bi} is the built-in potential; N_D is the doping concentration; A is the area; and C is the capacitance. In the reverse region, $1/C^2$ vs. V gave a straight line from which we calculated the flat band voltage V_0 (intercept of x-axis) and built-in potential V_{bi}. The barrier height can be calculated by the below expression,

$$V_n = E_C - E_F = \frac{kT}{q} In\left(\frac{N_C}{N_D}\right) \tag{4}$$

where E_C and E_F represent the conduction band minima and Fermi energy level, respectively. We used a N_C (effective density of states in the conduction band) of 1.7×10^{18} cm^{-3} [34]. Schottky barrier height can be expressed as

$$\phi_b = V_{bi} + V_n + \frac{kT}{q} \tag{5}$$

From the C–V measurement, a Schottky barrier height value was obtained at 0.59 eV and 0.48 eV in Ni/Au and Pt/Ti/Pt/Au, respectively. Apparently, this was high compared to the I–V measured values [35] which is shown in Table 1.

Table 1. Comparison of I–V and C–V measured data of both devices at room temperature.

Schottky Barrier Height (ϕ_b) (eV)	I–V Method	C–V Method
Ni/Au	0.55	0.59
Pt/Ti/Pt/Au	0.45	0.48

The transconductance showed almost similar characteristics of both devices at the same gate length of 14 um. The drain current in the Pt/Ti/Pt/Au device in Figure 4b was slightly lower than the Ni/Au gated device, indicating that the 2DEG carrier concentration below the gate area had decreased [7]. The transfer characteristics of the Ni/Au and Pt/Ti/Pt/Au contacts on the AlGaN/GaN HEMTs are shown in Figure 4a. The off-state leakage current of the Pt/Ti/Pt/Au HEMT was slightly higher than that of the Ni/Au HEMT. In the voltage region below −1.5 V, the Pt-based Schottky gate yielded a high forward leakage current. Extra tunneling of the currents has been suggested in the Pt gate due to the surface level of the MS state, as demonstrated by Zhang et al. (2006) [36]. Thus, the leakage current increased instead of reducing at the minimum forward bias.

In Figure 5, the critical voltage of the Ni/Au HEMT, followed by a sudden increase in the gate leakage current, was about −25 V, which resulted in permanent defect sites at the MS interface. This sudden increase in the gate leakage current can be ascribed to the inverse piezoelectric effect [37]. In contrast, no sudden increase in the gate leakage current was observed up to −60 V in the Pt/Ti/Pt/Au HEMT [38]. Although all characteristics of the Pt/Ti/Pt/Au HEMT including Schottky diode, transistor I–V, and C–V measurements, showed significant improvements in the forward region, the device characteristics in the reverse region were degraded due to the inhomogeneities at the MS interface.
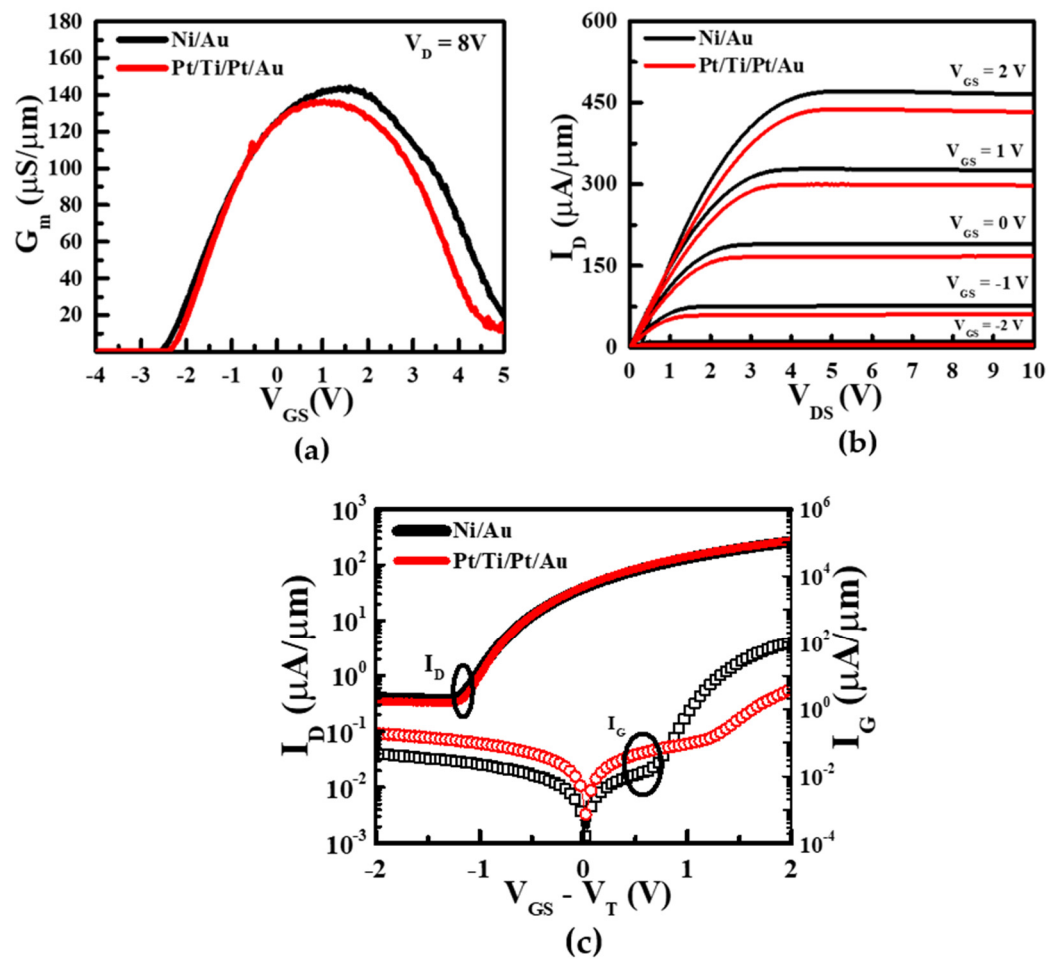
Figure 4. (**a**)Transconductance characteristics, (**b**) Output characteristics at different gate voltage and (**c**) transfer characteristics of Ni/Au and Pt/Ti/Pt/Au on AlGaN/GaN HEMTs with VD fixed at 8 V.
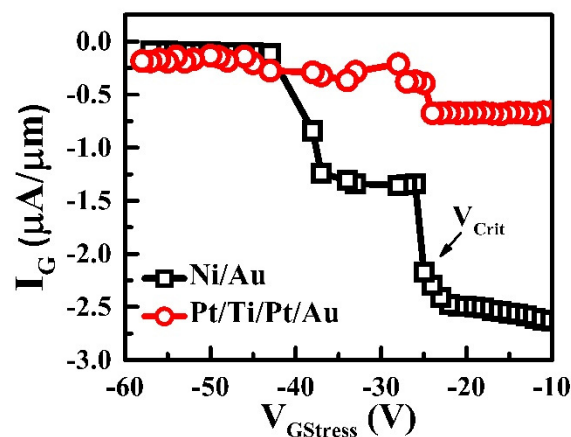

Figure 5. Critical voltages (V_{crit}) of Ni/Au and Pt/Ti/Pt/Au on AlGaN/GaN HEMTs in the range of −10 to −60 V with stepped stresses. The V_{crit} of Ni/Au was about −25 V and that of Pt/Ti/Pt/Au was unspecified for up to −60 V.

3.2. Reliability Instability Based on Temperature

To verify the degradation of the SBH from high electrical stress, the forward and reverse leakage currents of the Ni/Au and Pt/Ti/Pt/Au contacts on the AlGaN/GaN HEMTs were evaluated before and after off-state stress application (V_D = 50 V, V_G = −7 V) over a duration of 3600 s. The reverse leakage current of the Pt/Ti/Pt/Au contact after

off-state stress application showed a greater reduction than that of the initial device while that of the Ni/Au increased, as shown in Figure 6. It is also interesting to note that the SBHs of the Ni/Au and Pt/Ti/Pt/Au after application of off-state stress decreased from 0.55 to 0.49 eV and increased from 0.46 to 0.69 eV, respectively. This means that the hot carriers under the off-state stress have a significantly effect on the MS. In fact, the stress condition at room temperature (25 °C) depends significantly on the gate voltage and electric field. The metallization schemes for the Schottky contacts on the AlGaN/GaN HEMT must thus be verified for thermal instabilities due to the Ga out-diffusion and Au interdiffusion at elevated temperatures.
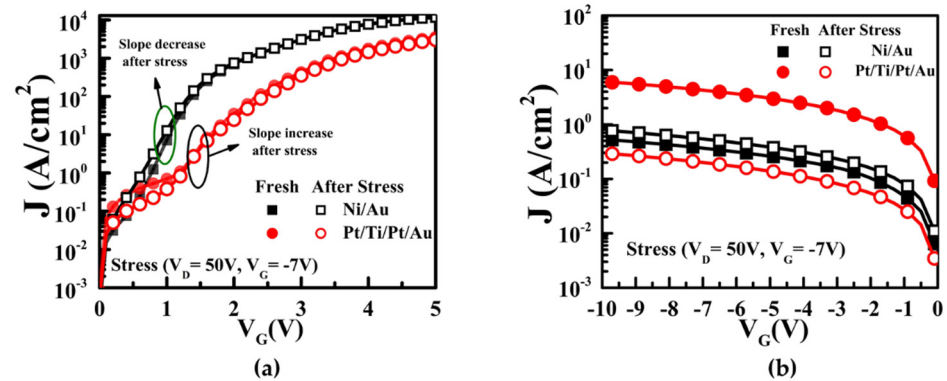

Figure 6. (**a**) Forward leakage current and (**b**) reverse leakage current of Ni/Au and Pt/Ti/Pt/Au on AlGaN/GaN HEMTs before and after off-state stress ($V_D = 50$ V, $V_G = -7$ V) during 3600 s.

The thermal reliability instabilities for the Ni/Au and Pt/Ti/Pt/Au HEMTs were examined in the temperature range of 298 to 368 K in intervals of 10 K. Figure 7 shows the J–V characteristics of the Ni/Au and Pt/Ti/Pt/Au contacts after application of off-state stress ($V_D = 50$ V, $V_G = -7$ V) at different temperatures. The reverse leakage currents of the Ni/Au HEMT before and after off-state stressing at 298 K were not degraded; in fact, the off-state stress with increasing temperature caused greater initial-parameter degradation rather than at room temperature [39], as shown in Figure 7a, which can easily generate more interface traps. In contrast, the reverse leakage currents of the Pt/Ti/Pt/Au HEMT decreased after off-state stressing at 298 K, with further reduction at 308 K under the same off-state stress conditions.
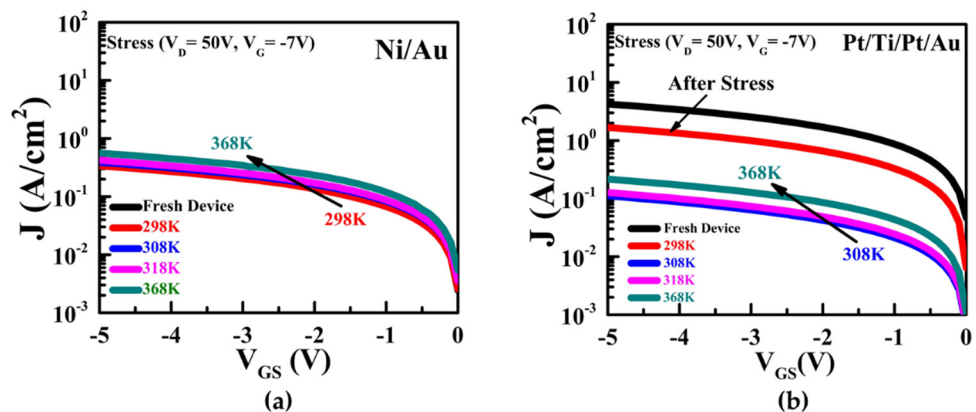

Figure 7. Reverse leakage current of the (**a**) Ni/Au and (**b**) Pt/Ti/Pt/Au on AlGaN/GaN HEMTs after off-state stress ($V_D = 50$ V, $V_G = -7$ V) in the temperature range of 298 K to 368 K measured at a temperature interval of 10 K. [Curves are not shown from 328 K to 358 K].

To investigate the barrier height and ideality factor of both devices, we repeated the same experiment with both Ni/Au and Pt/Ti/Pt/Au with different gate lengths of 10 μm and increased the temperature beyond 368 K to observe the degradation effect [40–43].

Figure 8a demonstrates the stress with temperature effect carried out on both devices. Barrier height of Ni/Au increased in a conventional way and the device burnt out at a 368 K temperature with the same off-state stress applied (V_D = 50 V, V_G = −7 V). The Pt/Ti/Pt/Au gated device had no breakdown issues after a temperature of 368 K. It was difficult to compare the ideality factor at a higher gate length (14 μm) due to high leakage current; therefore, we narrowed it down with shorter gate devices. We found a better ideality factor at a gate length of 10 μm compared to the gate length of 14 μm. Due to the high gate leakage current, the ideality factor (4.3) was high in Pt/Ti/Pt/Au [44,45]. However, after stress at 308 K, the ideality factor decreased, and was between 1 and 2 as the temperature increased.
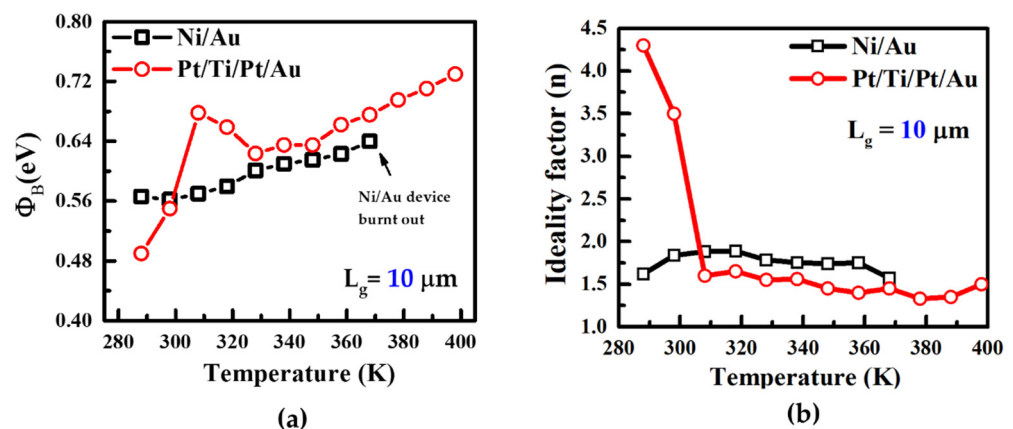

Figure 8. Barrier height (**a**) and ideality factor (**b**) of the Ni/Au and Pt/Ti/Pt/Au devices in the same experiment described in Figure 7. Ni/Au gated device burnt out after 378 K (**a**) and there was an increase in Schottky barrier height from 0.49 eV to 0.68 eV at 308 K in the Pt/Ti/Pt/Au gated device.

Although the initial characteristics of the Pt/Ti/Pt/Au HEMT were determined by the inhomogeneities at the MS interface, the interfacial trap states can be reduced by curing the surface donor state of the Pt-based Schottky contact after off-state stressing. For an increase in temperature over 308 K under the same off-state stress condition, the reverse leakage current degradation is mitigated by the inverse piezoelectric effect mechanism. As the temperature increases further, the number of electrons with very high energies decreases. At increased temperature, greater phonon-induced carrier scattering mitigates carrier acceleration, which minimizes hot-carrier damage [46].

In other words, the number of moderate-energy carriers (0.5 eV to 2.5 eV) increases with an increase in temperature. Moderate-energy carriers could produce or reorganize flaws in the MS contacts after application of off-state stress if the defect activation energies are sufficiently low. Thus, it is necessary to analyze the concurrent SBH and hot-carrier degradation because of the interfacial trap states at the MS contacts.

4. Conclusions

Detailed reliability assessments and electrical characterizations were performed for Ni/Au and Pt/Ti/Pt/Au gate contacts on AlGaN/GaN HEMTs. Although the Pt-based gate was expected to have a high work function when used on top of the AlGaN, the SBH and reverse leakage current degraded in comparison with those of the Ni-based gate, implying that the high-energy Pt atoms induced surface roughness during the e-beam evaporation process. After applying off-state stresses and high temperatures, Pt/Ti/Pt/Au HEMTs showed abrupt reductions in the reverse leakage currents, which improved the SBH by suppressing the interfacial donor states. From the behaviors of the interfacial trap states of the MS contacts, the stability of the AlGaN/GaN HEMT could be ascertained by simultaneously investigating the SBH and reliability instability.

References

1. del Alamo, J.A.; Joh, J. GaN HEMT reliability. *Microelectron. Reliab.* **2009**, *49*, 1200–1206. [CrossRef]
2. Nguyen, C. MODFETs MBE. *Electron. Lett.* **2000**, *36*, 468–469. [CrossRef]
3. Sun, H.; Alt, A.R.; Member, S.; Benedickter, H.; Feltin, E.; Carlin, J.; Gonschorek, M.; Grandjean, N.; Bolognesi, C.R.; We, A.; et al. 205-GHz (Al,In)N/GaN HEMTs. *IEEE Electron Device Lett.* **2010**, *31*, 957–959. [CrossRef]
4. Wang, W.; Derluyn, J.; Germain, M.; Leys, M.; Degroote, S.; Schreurs, D.; Borghs, G. Effect of surface passivation on two-dimensional electron gas carrier density in AlGaN/GaN structures. *Jpn. J. Appl. Phys. Part 2 Lett.* **2006**, *45*, 43–46. [CrossRef]
5. Feng, Z.; Zhou, Y.; Cai, S.; Lau, K.M. Doping concentration and structural dependences of the thermal stability of the 2DEG in GaN-based high-electron-mobility transistor structures. *Jpn. J. Appl. Phys. Part 2 Lett.* **2005**, *44*, 2–5. [CrossRef]
6. Ambacher, O.; Foutz, B.; Smart, J.; Shealy, J.R.; Weimann, N.G.; Chu, K.; Murphy, M.; Sierakowski, A.J.; Schaff, W.J.; Eastman, L.F.; et al. Two dimensional electron gases induced by spontaneous and piezoelectric polarization in undoped and doped AlGaN/GaN heterostructures. *J. Appl. Phys.* **2000**, *87*, 334–344. [CrossRef]
7. Visvkarma, A.K.; Sharma, C.; Laishram, R.; Kapoor, S.; Rawal, D.S.; Vinayak, S.; Saxena, M. Comparative study of Au and Ni/Au gated AlGaN/GaN high electron mobility transistors. *AIP Adv.* **2019**, *9*, 125231. [CrossRef]
8. Mimouni, A.; Fernández, T.; Rodriguez-Tellez, J.; Tazon, A.; Baudrand, H.; Boussuis, M. Gate Leakage Current in GaN HEMT's: A Degradation Modeling Approach. *Electr. Electron. Eng.* **2013**, *2*, 397–402. [CrossRef]
9. Zhu, J.; Hou, B.; Chen, L.; Zhu, Q.; Yang, L.; Zhou, X.; Zhang, P.; Ma, X.; Hao, Y. Threshold Voltage Shift and Interface/Border Trapping Mechanism in Al_2O_3/AlGaN/GaN MOS-HEMTs. In Proceedings of the 2018 IEEE International Reliability Physics Symposium (IRPS), Burlingame, CA, USA, 11–15 March 2018; pp. 2018–2021.
10. Jimenez, J.L.; Chowdhury, U. X-band GaN fet reliability. *IEEE Int. Reliab. Phys. Symp.* **2008**, 429–435. [CrossRef]
11. Besendörfer, S.; Meissner, E.; Medjdoub, F.; Derluyn, J.; Friedrich, J.; Erlbacher, T. The impact of dislocations on AlGaN/GaN Schottky diodes and on gate failure of high electron mobility transistors. *Sci. Rep.* **2020**, *10*, 1–12. [CrossRef]
12. Chowdhury, U.; Jimenez, J.L.; Lee, C.; Beam, E.; Saunier, P.; Balistreri, T.; Park, S.Y.; Lee, T.; Wang, J.; Kim, M.J.; et al. TEM observation of crack- and pit-shaped defects in electrically degraded GaN HEMTs. *IEEE Electron Device Lett.* **2008**, *29*, 1098–1100. [CrossRef]
13. Jungwoo, J.; Del Alamo, J.A. Mechanisms for electrical degradation of GaN high-electron mobility transistors. In Proceedings of the 2006 International Electron Devices Meeting, San Francisco, CA, USA, 11–13 December 2006; pp. 5–8. [CrossRef]
14. Astre, G.; Tartarin, J.G.; Lambert, B. Trapping related degradation effects in AlGaN/GaN HEMT. In Proceedings of the The 5th European Microwave Integrated Circuits Conference, Paris, France, 27–28 September 2010; pp. 298–301.
15. Meneghesso, G.; Verzellesi, G.; Danesin, F.; Rampazzo, F.; Zanon, F.; Tazzoli, A.; Meneghini, M.; Zanoni, E. Reliability of GaN high-electron-mobility transistors: State of the art and perspectives. *IEEE Trans. Device Mater. Reliab.* **2008**, *8*, 332–343. [CrossRef]
16. Hoon Shin, J.; Je Jo, Y.; Kim, K.C.; Jang, T.; Sang Kim, K. Gate metal induced reduction of surface donor states of AlGaN/GaN heterostructure on Si-substrate investigated by electroreflectance spectroscopy. *Appl. Phys. Lett.* **2012**, *100*, 111908. [CrossRef]
17. Yu, C.H.; Luo, Q.Z.; Luo, X.D.; Liu, P.S. Donor-like surface traps on two-dimensional electron gas and current collapse of AlGaN/GaN HEMTs. *Sci. World J.* **2013**, *2013*, 931980. [CrossRef]
18. Shin, J.H.; Park, J.; Jang, S.; Jang, T.; Sang Kim, K. Metal induced inhomogeneous Schottky barrier height in AlGaN/GaN Schottky diode. *Appl. Phys. Lett.* **2013**, *102*, 1–6. [CrossRef]
19. Suzuki, A.; Akira, K.; Asubar, J.T.; Tokuda, H.; Kuzuhara, M. Improved current collapse in AlGaN/GaN HEMTs with 3-dimensional field plate structure. *IMFEDK 2015–2015 Int. Meet. Futur. Electron Devices Kansai* **2015**, *31*, 36–37. [CrossRef]
20. Long, W.; Ou, H.; Kuo, J.; Chin, K.K. Dual-Material Gate (DMG) Field Effect Transistor. *IEEE Electron Device Lett.* **1999**, *46*, 865–870. [CrossRef]
21. Green, R.T.; Luxmoore, I.J.; Lee, K.B.; Houston, P.A.; Ranalli, F.; Wang, T.; Parbrook, P.J.; Uren, M.J.; Wallis, D.J.; Martin, T. Characterization of gate recessed GaN/AlGaN/GaN high electron mobility transistors fabricated using a SiCl4/SF6 dry etch recipe. *J. Appl. Phys.* **2010**, *108*, 013711. [CrossRef]
22. Laurent, M.A.; Gupta, G.; Suntrup, D.J.; DenBaars, S.P.; Mishra, U.K. Barrier height inhomogeneity and its impact on (Al,In,Ga)N Schottky diodes. *J. Appl. Phys.* **2016**, *119*, 064501. [CrossRef]

23. Meneghesso, G.; Meneghini, M.; Stocco, A.; Bisi, D.; de Santi, C.; Rossetto, I.; Zanandrea, A.; Rampazzo, F.; Zanoni, E. Degradation of AlGaN/GaN HEMT devices: Role of reverse-bias and hot electron stress. *Microelectron. Eng.* **2013**, *109*, 257–261. [CrossRef]

24. Mishra, U.K.; Shen, L.; Kazior, T.E.; Wu, Y.F. GaN-based RF power devices and amplifiers. *Proc. IEEE* **2008**, *96*, 287–305. [CrossRef]

25. Mukherjee, S.; Puzyrev, Y.; Chen, J.; Fleetwood, D.M.; Schrimpf, R.D.; Pantelides, S.T. Hot-Carrier Degradation in GaN HEMTs Due to Substitutional Iron and Its Complexes. *IEEE Trans. Electron Devices* **2016**, *63*, 1486–1494. [CrossRef]

26. Zhang, T.; Wang, Y.; Zhang, Y.; Lv, Y.; Ning, J.; Zhang, Y.; Zhou, H.; Duan, X.; Zhang, J.; Hao, Y. Comprehensive Annealing Effects on AlGaN/GaN Schottky Barrier Diodes with Different Work-Function Metals. *IEEE Trans. Electron Devices* **2021**, *68*, 2661–2666. [CrossRef]

27. Schmitz, A.C.; Ping, A.T.; Asif Khan, M.; Chen, Q.; Yang, J.W.; Adesida, I. Metal contacts to n-type GaN. *J. Electron. Mater.* **1998**, *27*, 255–260. [CrossRef]

28. Hashizume, T.; Hasegawa, H. Effects of nitrogen deficiency on electronic properties of AlGaN surfaces subjected to thermal and plasma processes. *Appl. Surf. Sci.* **2004**, *234*, 387–394. [CrossRef]

29. Hasegawa, H.; Inagaki, T.; Ootomo, S.; Hashizume, T. Mechanisms of current collapse and gate leakage currents in AlGaN/GaN heterostructure field effect transistors. *J. Vac. Sci. Technol. B Microelectron. Nanom. Struct.* **2003**, *21*, 1844. [CrossRef]

30. Iucolano, F.; Roccaforte, F.; Giannazzo, F.; Raineri, V. Barrier inhomogeneity and electrical properties of PtGaN Schottky contacts. *J. Appl. Phys.* **2007**, *102*, 113701. [CrossRef]

31. Hashizume, T.; Kotani, J.; Hasegawa, H. Leakage mechanism in GaN and AlGaN Schottky interfaces. *Appl. Phys. Lett.* **2004**, *84*, 4884–4886. [CrossRef]

32. Ahn, W.; Seok, O.; Ha, M.-W.; Kim, Y.-S.; Han, M.-K. Various Schottky Contacts of AlGaN/GaN Schottky Barrier Diodes. In Proceedings of the ECS Meeting, San Francisco, CA, USA, 27 October–1 November 2013.

33. Sze, S.M. *Physics of Semiconductor Devices*; Wiely: New York, NY, USA, 2006; ISBN 9780471143239.

34. Potthast, S. *Growth and Characterization of Cubic AlGaN/GaN Based Devices*; der Universitat Paderborn: Paderborn, Germany, 2006.

35. Bhattacharyya, A.; Ranga, P.; Saleh, M.; Roy, S.; Scarpulla, M.A.; Lynn, K.G.; Krishnamoorthy, S. Schottky Barrier Height Engineering in β-Ga2O3 Using SiO2 Interlayer Dielectric. *IEEE J. Electron Devices Soc.* **2020**, *8*, 286–294. [CrossRef]

36. Zhang, H.; Miller, E.J.; Yu, E.T. Analysis of leakage current mechanisms in Schottky contacts to GaN and Al 0.25Ga 0.75N/GaN grown by molecular-beam epitaxy. *J. Appl. Phys.* **2006**, *99*. [CrossRef]

37. Joh, J.; Xia, L.; del Alamo, J.A. Gate current degradation Mechanisms of GaN High Electron Mobility Transistors. In Proceedings of the IEEE Electron Device Meeting, Washington, DC, USA, 10–12 December 2007; pp. 385–388. [CrossRef]

38. Lo, C.-F.; Liu, L.; Kang, T.-S.; Davies, R.; Gila, B.P.; Pearton, S.J.; Kravchenko, I.I.; Laboutin, O.; Cao, Y.; Johnson, W.; et al. Improved Off-State Stress Critical Voltage on AlGaN/GaN High Electron Mobility Transistors Utilizing Pt/Ti/Au Based Gate Metallization. *ECS Trans.* **2019**, *41*, 63–70. [CrossRef]

39. Heremans, P.; Van Den Bosch, G.; Bellens, R.; Groeseneken, G.; Maes, H.E. Temperature Dependence of the Channel Hot-Carrier Degradation of n-Channel MOSFET's. *IEEE Trans. Electron Devices* **1990**, *37*, 980–993. [CrossRef]

40. Ravinandan, M.; Rao, P.K.; Rajagopal Reddy, V. Analysis of the current-voltage characteristics of the Pd/Au Schottky structure on n-type GaN in a wide temperature range. *Semicond. Sci. Technol.* **2009**, *24*, 035004. [CrossRef]

41. Karboyan, S.; Tartarin, J.; Lambert, B.; Karboyan, S.; Tartarin, J.; Analysis, B.L.; Gan, A.; Karboyan, S.; Tartarin, J.G.; Lambert, B. Analysis of Barrier Inhomogeneities in AlGaN/GaN HEMTs' Schottky Diodes by I-V-T measurements To cite this version: HAL Id: Hal-01343345 Analysis of Barrier Inhomogeneities in AlGaN/GaN HEMTs' Schottky Diodes by I-V-T measurements. In Proceedings of the 2013 European Microwave Integrated Circuit Conference, Nuremberg, Germany, 6–8 October 2013.

42. Garg, M.; Kumar, A.; Nagarajan, S.; Sopanen, M.; Singh, R. Investigation of significantly high barrier height in Cu/GaN Schottky diode. *AIP Adv.* **2016**, *6*, 015206. [CrossRef]

43. Arehart, A.R.; Moran, B.; Speck, J.S.; Mishra, U.K.; DenBaars, S.P.; Ringel, S.A. Effect of threading dislocation density on Ni/n-GaN Schottky diode I-V characteristics. *J. Appl. Phys.* **2006**, *100*, 1–8. [CrossRef]

44. Lee, K.B.; Parbrook, P.J.; Wang, T.; Bai, J.; Ranalli, F.; Airey, R.J.; Hill, G. The origin of the high ideality factor in AlGaN-based quantum well ultraviolet light emitting diodes. *Phys. Status Solidi Basic Res.* **2010**, *247*, 1761–1763. [CrossRef]

45. Shah, J.M.; Li, Y.L.; Gessmann, T.; Schubert, E.F. Experimental analysis and theoretical model for anomalously high ideality factors (n ≫ 2.0) in AlGaN/GaN p-n junction diodes. *J. Appl. Phys.* **2003**, *94*, 2627–2630. [CrossRef]

46. Cheney, D.J.; Douglas, E.A.; Liu, L.; Lo, C.F.; Xi, Y.Y.; Gila, B.P.; Ren, F.; Horton, D.; Law, M.E.; Smith, D.J.; et al. Reliability studies of AlGaN/GaN high electron mobility transistors. *Semicond. Sci. Technol.* **2013**, *28*, 074019. [CrossRef]